Room temperature detection of sub-terahertz radiation in double-grating-gate transistors

著者	Coquillat D., Nadar S., Teppe F., Dyakonova N., Boubanga-Tombet S., Knap W., Nishimura T., Otsuji T., Meziani Y. M., Tsymbalov G. M., Popov V. V.
journal or publication title	Optics Express
volume	18
number	6
page range	6024-6032
year	2010
URL	http://hdl.handle.net/10097/52408

doi: 10.1364/OE.18.006024

Room temperature detection of sub-terahertz radiation in double-grating-gate transistors

D. Coquillat,[1,*] S. Nadar,[1] F. Teppe,[1] N. Dyakonova,[1] S. Boubanga-Tombet,[1] W. Knap[1], T. Nishimura,[2] T. Otsuji,[2,] Y. M. Meziani,[2,3] G. M. Tsymbalov,[4] and V. V. Popov[1,2,4,]

[1]*GES UMR5650, CNRS-Université Montpellier 2, 34095 Montpellier, France*
[2]*Research Institute of Electrical Communication, Tohoku University, 2-1-1 Katahira, Aoba-Ku, Sendai 980-8577, Japan*
[3]*Dpto. de Fisica Aplicada, Universidad de Salamanca, Pza de la Merced s/n, 37008 Salamanca, Spain*
[4]*Kotelnikov Institute of Radio Engineering and Electronics (Saratov Branch), 410019 Saratov, Russia*
**coquillat@ges.univ-montp2.fr*

Abstract: Room temperature photovoltaic non-resonant detection by large area double-grating-gate InGaP/InGaAs/GaAs heterostructures was investigated in sub-THz range (0.24 THz). Semi-quantitative estimation of the characteristic detection length combined with self-consistent calculations of the electric fields excited in the structure by incoming terahertz radiation allowed us to interpret quantitatively the results and conclude that this detection takes place mainly in the regions of strong oscillating electric field excited in depleted portions of the channel.

OCIS codes: (040.0040) Detectors; (040.1880) Detection; (040.2235) Far infrared or terahertz; (050.2770) Gratings; (250.5403) Plasmonics.

References and links

1. M. Dyakonov, and M. Shur, "Plasma wave electronics: novel terahertz devices using two dimensional electron fluid," IEEE Trans. Electron. Dev. **43**(10), 1640–1645 (1996).
2. W. Knap, V. Kachorovskii, Y. Deng, S. Rumyantsev, J.-Q. Lü, R. Gaska, M. S. Shur, G. Simin, X. Hu, M. Asif Khan, C. A. Saylor, and L. C. Brunel, "Nonresonant detection of terahertz radiation in field effect transistors," J. Appl. Phys. **91**(11), 9346–9353 (2002).
3. W. Knap, F. Teppe, Y. Meziani, N. Dyakonova, J. Lusakowski, F. Boeuf, T. Skotnicki, D. Maude, S. Rumyantsev, and M. S. Shur, "Plasma wave detection of sub-terahertz and terahertz radiation by silicon field-effect transistors," Appl. Phys. Lett. **85**(4), 675–677 (2004).
4. R. Tauk, F. Teppe, S. Boubanga, D. Coquillat, W. Knap, Y. M. Meziani, C. Gallon, F. Boeuf, T. Skotnicki, C. Fenouillet-Beranger, D. K. Maude, S. Rumyantsev, and M. S. Shur, "Plasma wave detection of terahertz radiation by silicon field effect transistors: responsivity and noise equivalent power," Appl. Phys. Lett. **89**(25), 253511 (2006).
5. W. Knap, Y. Deng, S. Rumyantsev, J.-Q. Lü, M. S. Shur, C. A. Saylor, and L. C. Brunel, "Resonant detection of subterahertz radiation by plasma waves in a submicron field-effect transistor," Appl. Phys. Lett. **80**(18), 3433–3435 (2002).
6. W. Knap, Y. Deng, S. Rumyantsev, and M. S. Shur, "Resonant detection of subterahertz and terahertz radiation by plasma waves in submicron field-effect transistors," Appl. Phys. Lett. **81**(24), 4637–4639 (2002).
7. A. El Fatimy, F. Teppe, N. Dyakonova, W. Knap, D. Seliuta, G. Valušis, A. Shchepetov, Y. Roelens, S. Bollaert, A. Cappy, and S. Rumyantsev, "Resonant and voltage-tunable terahertz detection in InGaAs/InP nanometer transistors," Appl. Phys. Lett. **89**(13), 131926 (2006).
8. S. J. Allen, Jr., D. S. Tsui, and R. A. Logan, "Observation of the two-dimensional plasmon in silicon inversion layers," Phys. Rev. Lett. **38**(17), 980–983 (1977).
9. T. N. Theis, "Plasmons in inversion layers," Surf. Sci. **98**(1-3), 515–532 (1980).
10. E. Batke, D. Heitmann, and C. W. Tu, "Plasmon and magnetoplasmon excitation in two-dimensional electron space-charge layers on GaAs," Phys. Rev. B **34**(10), 6951–6960 (1986).
11. V. V. Popov, M. S. Shur, G. M. Tsymbalov, and D. V. Fateev, "Higher-order plasmon resonances in GaN field-effect transistor arrays," Int. J. High Speed Electron. Syst. **17**(03), 557–566 (2007).
12. V. V. Popov, O. V. Polischuk, T. V. Teperik, X. G. Peralta, S. J. Allen, N. J. M. Horing, and M. C. Wanke, "Absorption of terahertz radiation by plasmon modes in a grid-gated double-quantum-well field-effect transistor," J. Appl. Phys. **94**(5), 3556–3562 (2003).
13. X. G. Peralta, S. J. Allen, M. C. Wanke, N. E. Harff, J. A. Simmons, M. P. Lilly, J. L. Reno, P. J. Burke, and J. P. Eisenstein, "Terahertz photoconductivity and plasmon modes in double-quantum-well field-effect transistors," Appl. Phys. Lett. **81**(9), 1627–1629 (2002).
14. E. A. Shaner, M. Lee, M. C. Wanke, A. D. Grine, J. L. Reno, and S. J. Allen, "Single-quantum-well grating-gated terahertz plasmon detectors," Appl. Phys. Lett. **87**(19), 193507 (2005).

#119947 - $15.00 USD Received 13 Nov 2009; revised 18 Dec 2009; accepted 18 Dec 2009; published 11 Mar 2010

15. T. Otsuji, M. Hanabe, T. Nishimura, and E. Sano, "A grating-bicoupled plasma-wave photomixer with resonant-cavity enhanced structure," Opt. Express **14**(11), 4815–4825 (2006), http://www.opticsinfobase.org/oe/abstract.cfm?URI=oe-14-11-4815.
16. T. Otsuji, Y. M. Meziani, M. Hanabe, T. Ishibashi, T. Uno, and E. Sano, "Grating-bicoupled plasmon-resonant terahertz emitter fabricated with GaAs-based heterostructure material systems," Appl. Phys. Lett. **89**(26), 263502 (2006).
17. V. V. Popov, G. M. Tsymbalov, and M. S. Shur, "Plasma wave instability and amplification of terahertz radiation in field-effect-transistor arrays," J. Phys. Condens. Matter **20**(38), 384208 (2008).

1. Introduction

It is known that hydrodynamic nonlinearities in two-dimensional (2*D*) electron channels can be used for detection of terahertz (THz) radiation [1]. Resonant THz detection is related to the excitation of high quality plasma waves (plasmons) in 2*D* electron channel, whereas a broadband non-resonant THz detection is related to overdamped plasmons in depleted regions of the channel. In the both resonant and non-resonant cases, THz photoresponse originates from the nonlinear dynamics of 2*D* electron fluid described by the hydrodynamic equations [1]

$$\frac{\partial V(x,t)}{\partial t} + V(x,t)\frac{\partial V(x,t)}{\partial x} + \frac{V(x,t)}{\tau} + \frac{e}{m^*}E(x,t) = 0, \tag{1}$$

$$e\frac{\partial}{\partial t}N(x,t) - \frac{\partial}{\partial x}j(x,t) = 0, \tag{2}$$

where $E(x,t)$ is the in-plane electric field depending on the time t and coordinate x in 2*D* electron system, τ is the electron momentum relaxation time, $j(x,t) = -eN(x,t)V(x,t)$ is the density of induced electric current, $N(x,t)$ and $V(x,t)$ are hydrodynamic electron density and velocity in 2*D* electron channel, and e and m^* are the electron charge and effective mass, respectively. There are two different nonlinear terms in the system Eqs. (1) and (2): the second term in the Euler equation Eq. (1) describing the nonlinear electron convection in 2*D* electron fluid and the product $N(x,t)V(x,t)$ defining the current density in the continuity equation Eq. (2). Time average of the nonlinear current yields the detection signal. It should be noted that either of the two nonlinear terms vanishes in the case of uniform oscillating currents flowing in 2*D* system. Hence, those nonlinearities are related to non-uniform currents inherent in the plasmon mode. In principle, both nonlinear terms can contribute to the detection signal depending on the geometry of the structure and the length of 2*D* electron channel. However, for symmetry reasons, the detection response must be zero in 2*D* electron channel with identical boundary conditions at its opposite ends if there is no bias DC current flowing in the channel. As shown in [1,2], the nonlinear electron convection does not contribute to a non-resonant detection signal for relatively long 2*D* electron channel (when the length of the sample is much longer than the plasmon correlation length). Both the non-resonant [2–4] and resonant [5–7] plasmon detection have been observed experimentally in single-unit field-effect transistors with 2*D* electron channels.

It can be anticipated that high net detectivity can be obtained if a high-quality plasmon resonance is excited in the resonant plasmonic THz detector, while high net detectivity of the non-resonant THz detector can be obtained if strong THz electric fields are induced in depleted regions of the channel. Therefore, the problem of effective coupling between THz radiation and 2*D* electron system is of crucial importance. The metal grating coupler is a conventional tool that can ensure strong coupling between the plasmons in 2*D* electron channel and THz radiation [8–12]. Resonant plasmon THz detection based on the photoconductive and photovoltaic response of the grating-gated field-effect-transistor structures was reported in [13,14].

In this paper, we report on the room temperature non-resonant THz detection in large area double-grating-gate InGaP/InGaAs/GaAs transistors and interpret this detection as coming from the regions of strong oscillating electric field excited in depleted portions of the channel.

#119947 - $15.00 USD Received 13 Nov 2009; revised 18 Dec 2009; accepted 18 Dec 2009; published 11 Mar 2010

2. Experimental

The device structure is based on InGaP/InGaAs/GaAs high-electron mobility transistor (HEMT) and incorporates doubly interdigitated grating gates (*G*1 and *G*2) [15,16] (see Fig. 1). The 2*D* electron channel is formed in a quantum well at the heterointerface between a 15-nm-thick undoped InGaAs channel layer and a 60-nm-thick, Si-δ doped InGaP carrier-supplying layer. The electron density in the channel is 2.5×10^{12} cm^{-2} with the electron effective mass and room temperature mobility $m^*= 0.04m_0$ where m_0 is the free-electron mass, and $\mu =$ 7000 cm^2/V·s, respectively. The grating gate is formed with 65-nm-thick Ti/Au/Ti by a standard lift-off process. Four different structures with a double-grating-gate were fabricated. The metal fingers of one grating gate *G*1 are of the same length L_{G1} = 100 nm in all structures, while grating gate *G*2 was designed to have fingers of different lengths L_{G2} = 300, 800, 1300, and 1800 nm for different structures. The spacing between the grating-gate fingers is 100 nm for all four structures. We estimated the gate-to-channel separation as d = 65 nm. Side (source and drain) ohmic contacts of the device were fabricated which allowed us to apply DC drain bias voltage and to measure THz photoresponse. The whole length of the channel between the source and drain contacts covered by the double-grating gate is about 80 μm with the channel width of 30 μm in each structure. In different structures, double-grating gates have from 40 to 150 periods depending on the length of the period in a particular structure.

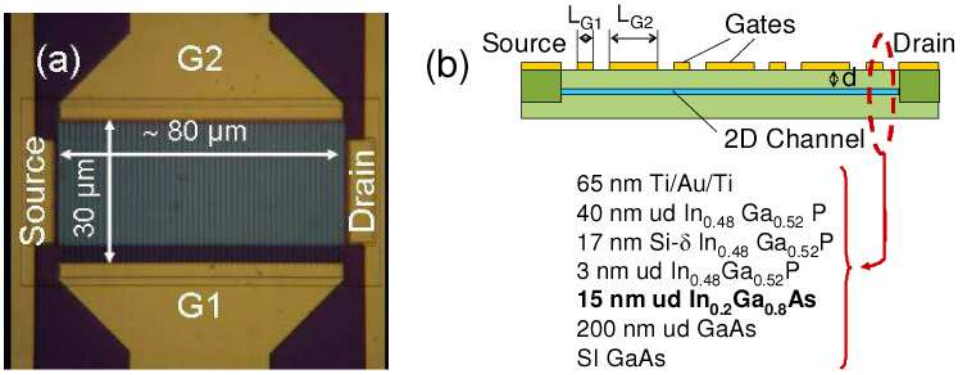

Fig. 1. (a) Top view and (b) schematic side view of the double-grating-gate device with indicated hétérostructure material systems. The external terahertz radiation is incident normally from the top.

The transfer characteristics of the structure with L_{G2} = 300 nm are shown in the inset of Fig. 2 for drain-to-source voltage 0.5 V. For these measurements, the source contact of the device was grounded and the 2*D* electron channel was depleted by applying negative voltage to either grating gate while leaving the other unbiased (grounded). The channel depletion threshold voltages estimated from Fig. 2 are $U_{thG1} \approx$–3.5 V and $U_{thG2} \approx$–3.0 V for biased gratings *G*1 and *G*2, respectively.

Each double-grating-gate structure was irradiated at normal incidence by THz beam at frequency 0.24 THz. We measured a photovoltaic DC response between the source and drain contacts (the source contact was grounded and no drain bias DC voltage was applied) at room temperature. The electron momentum relaxation time in 2D electron channel at T = 300 K is $\tau_m = \mu m^*/e$ = 0.17 ps, which yields the quality factor smaller than unity, $\omega\tau$ = 0.25, for the incident radiation frequency $\omega/2\pi$ = 0.24 THz. Therefore, the non-resonant detection should be expected in our experiments at room temperature. Terahertz radiation was generated by a Backward Wave Oscillator (BWO) with maximum output power of 5 mW. The radiation was linearly polarized and chopped at 170 Hz. The radiation-induced photovoltage ΔU was measured as a function of the gate voltage U_{G1} or/and U_{G2} as 170 Hz ac voltage component of the source-to-drain voltage using the standard lock-in technique. No special antenna was used

#119947 - $15.00 USD Received 13 Nov 2009; revised 18 Dec 2009; accepted 18 Dec 2009; published 11 Mar 2010

to couple THz radiation to the device. The sample holder was mounted on a rotary stage so that dependence of the signal on the polarization of the electric field of the incident THz wave in the sample plane could be measured.

Figure 2 demonstrates the photoresponse measured as a function of the gate voltage U_{G1} (for $U_{G2} = 0$) and that as a function of the gate voltage U_{G2} (for $U_{G1} = 0$) for the structure with $L_{G2} = 300$ nm when the THz electric field was directed across the grating-gate fingers (i.e., in the source-to-drain direction). The photoresponse grows when one of the grating gates, either $G1$ or $G2$, is biased to the threshold voltage.

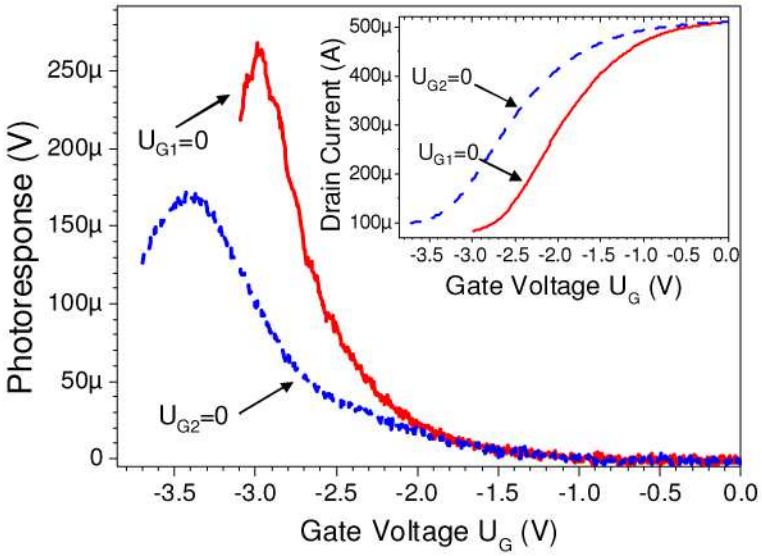

Fig. 2. The photoresponse at 0.24 THz in the structure with L_{G2}= 300 nm as a function of the gate voltage U_{G1} (for $U_{G2} = 0$) and as a function of the gate voltage U_{G2} (for $U_{G1} = 0$). The inset shows the transfer characteristics of the double-grating-gate transistor structure.

The strongest photoresponse in all structures was observed when the electric-field vector of the incident THz wave was directed across the grating-gate fingers (i.e., in the source-to-drain direction). Figure 3 shows the dependence of the photoresponse on the azimuthal angle φ between the THz electric field and the source-to-drain direction for the structure with L_{G2} = 1300 nm. A two-lobe-shape angle dependence that relatively well follows the $\cos^2\varphi$ law, was obtained with the maximal photoresponse for $\varphi = 0$. This demonstrates that the coupling between THz radiation and 2D electron channel is ensured by the double-grating gate.

#119947 - $15.00 USD Received 13 Nov 2009; revised 18 Dec 2009; accepted 18 Dec 2009; published 11 Mar 2010

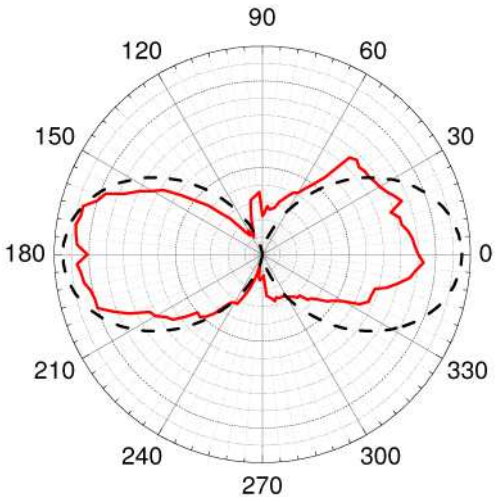

Fig. 3. Photoresponse at 0.24 THz as a function of the azimuthal angle φ between the electric field vector of the incident THz wave and the source-to-drain direction (solid curve). It follows the $\cos^2(\varphi)$ dependence (dashed curve) with the strongest photoresponse occurred for $\varphi = 0$.

Measured photoresponse per period of the structure for $\varphi = 0$ is documented in Table 1 for all four structures under two different biasing conditions. Within the measurement uncertainty, the photoresponse grows with decreasing the length of undepleted portion of the channel per the structure period (under unbiased grating-gate finger) for samples # 1-4, while it grows with increasing the length of a depleted portion of the channel per the structure period (under a biased grating-gate finger) for samples # 5-8. Note that an absolute value of the photoresponse is relatively small because fabrication arrangements were not undertaken to bring designed asymmetry into the structure unit cell, which is required for ensuring the photovoltaic response. (For a device having a vertical plane of the mirror symmetry, the photovoltaic response is zero for symmetry reasons.) However, measured dependence of the photoresponse on the structure geometry suggests that there is some systematic, though small, asymmetry in the double-grating gate in all four structures.

Table 1. Measured photoresponse for different samples

Sample #	**1**	**2**	**3**	**4**	**5**	**6**	**7**	**8**
$L_{G\text{-biased}}$ (nm) /$L_{G\text{-unbiased}}$ (nm)	100 /1800	100 /1300	100 /800	100 /300	300 /100	800 /100	1300 /100	1800 /100
Photoresponse per period (μV)	0.5	0.4	0.6	1.15	1.8	2.1	2.3	2.85

3. Theoretical consideration and discussion

The theory of non-resonant terahertz detection due to hydrodynamic nonlinearity of the 2*D* electron fluid was initially proposed in [1] and then developed in more advanced form in [2] taking into account a finite electron temperature. However, this theory assumes asymmetric excitation of the channel, where a predefined THz electric field is applied at one end of the channel, and then it describes how this field propagates along the channel producing a photoresponse. Therefore, such theory cannot be used directly for quantitative analysis of the periodic structure under study, where the oscillating currents are excited in every point of the channel simultaneously by normally incident THz wave. Because of that in this paper we use a semi-quantitative approach for describing the THz photoresponse in the double-grating-gate structure.

In a periodic structure, the electron convection term in the Euler equation [the second term in Eq. (1)] does not contribute to the photoresponse of the entire structure incorporating many dozens of periods because the spatial average of this term over the structure period is zero.

#119947 - $15.00 USD Received 13 Nov 2009; revised 18 Dec 2009; accepted 18 Dec 2009; published 11 Mar 2010

Therefore, the only source of hydrodynamic nonlinearity in the periodic structure is the product $N(x,t)V(x,t)$ defining the current density in 2*D* electron fluid. Then, for relatively small perturbations $N(x,t)$ and $V(x,t)$, the time-independent photoresponse current density is $j_0 = -e\langle N(x)V(x)\rangle$, where $N(x)$ and $V(x)$ are the amplitudes of the linear perturbations of the oscillating electron density and velocity, respectively, (i.e., those proportional to the first power of the electric field in 2*D* channel) and the angular brackets denote the spatial averaging over the period of the structure. As mentioned in section 2, the photocurrent will be zero in the structure with symmetric unit cell (having a vertical plane of the mirror symmetry) for symmetry reasons even if this type of nonlinearity works. Therefore, a specific asymmetry of the structure unit cell should be considered in order to calculate the THz photovoltaic response. However, we can evaluate the strength of the nonlinearity in a semi-quantitative way even without considering a particular asymmetry of the structure. The oscillating electron density $N(x)$ in every x-point of the channel is proportional to the normal component of the electric field at that point, while the oscillating electron velocity $V(x)$ in every x-point is proportional to the in-plane component of the THz electric field at that point. Amplitudes of the in-plane, E_x, and normal, E_y, components of the electric field in the channel are proportional to each other because they are interrelated by the linear Maxwell equation (or Poisson equation in the electrostatic case). However, those components of the electric field are shifted in phase along the x-coordinate by $\pi/2$. Let us assume for simplicity that $N(x)$ and $V(x)$ have harmonic dependences on the x-coordinate. Than we can estimate this nonlinearity as

$$N(x)V(x) \approx \left|\frac{E_x}{E_0}\right|^2 \sin\left(\frac{2\pi}{\Delta}x\right)\cos\left(\frac{2\pi}{\Delta}x\right),$$

where $|E_x/E_0|$ is the electric-field enhancement factor (the ratio between the amplitudes of the induced in-plane electric field E_x in 2*D* electron channel and the electric field E_0 in the incident THz wave) and Δ is the spatial period of the induced electric field variation along the x-coordinate in 2*D* electron channel. As shown in Refs [1,2]. and clearly demonstrated in Fig. 2, the non-resonant detection response originates predominantly in depleted parts of the channel. Then we can describe the net effect of detection coming from a depleted portion of the channel (per the structure period) by the characteristic detection length

$$L_D = \left|\frac{E_x}{E_0}\right|^2 \int_0^w \sin\left(\frac{2\pi}{\Delta}x\right)\cos\left(\frac{2\pi}{\Delta}x\right)dx = \frac{\Delta}{4\pi}\left|\frac{E_x}{E_0}\right|^2 \sin^2\left(\frac{2\pi}{\Delta}w\right), \qquad (3)$$

where w is the length of the depleted part of the channel within the strong electric field region per the structure period. The value of L_D exhibits maximum for $w = \Delta/4$ when the maximal asymmetry of the electric-field distribution over the depleted portion of 2*D* electron channel takes place.

We calculated the normal and in-plane electric field distributions over the period of the structure in a first-principle electromagnetic approach described in Ref [17]. for all eight samples specified in Table 1. Distributions of the oscillating electric-field amplitudes over the structure period for samples # 1 and 8 are shown in Fig. 4. Naturally, nodes of the in-plane component of the electric field coincide with antinodes of the normal component of the electric field. Strong electric field with the electric-field-enhancement factor $|E_x/E_0| \approx 5$ is excited in the channel under the entire gate *G*1 when it is biased down to the threshold voltage U_{thG1} while $U_{thG2} = 0$. However, strong electric field with the electric-field-enhancement factor $|E_x/E_0| \approx 2.5$ is excited only near the edges of gate *G*2 when it is biased down to the threshold voltage U_{thG2} while $U_{thG2} = 0$ because a long gate finger *G*2 effectively screens the central part of the gated channel. The regions with strong electric field can be thought as having the length of $\Delta/2$. It means that each region of strong electric field can be viewed as

#119947 - $15.00 USD Received 13 Nov 2009; revised 18 Dec 2009; accepted 18 Dec 2009; published 11 Mar 2010

two oppositely-connected channels of length Δ/4, which are short-circuited at the center of this region but open-circuited at the ends of this region.

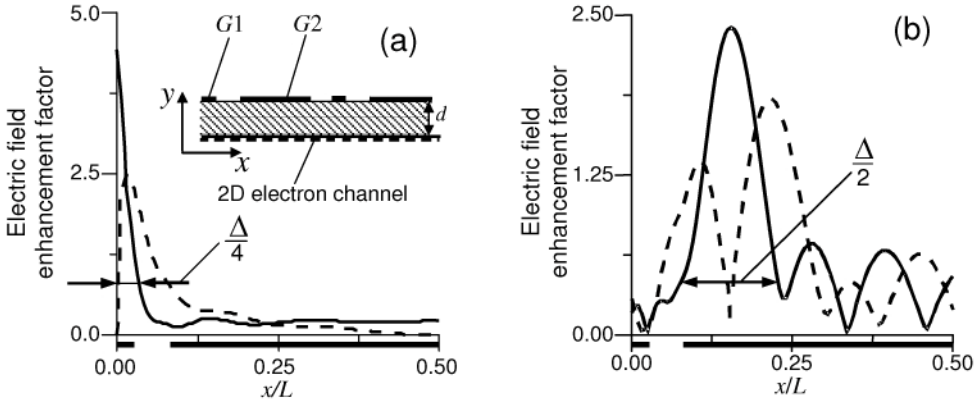

Fig. 4. In-plane (solid curves) and normal (dashed curves) THz electric field distributions in the 2*D* electron channel for (a) sample #1 and (b) sample #8 over a half of the structure period, *L*/2, at frequency 240 GHz. Inset in panel (a) shows a schematic of the double-grating-gate structure. Location of the grating-gate fingers is indicated by thick black bars under the abscissa axes. The origin is located under the centre of the *G*1 finger.

The widths of the regions with strong electric field, Δ/2, were estimated as 165 nm, 110 nm, 100 nm, 65 nm, 180 nm, 245 nm, 280 nm, and 330 nm for samples # 1 to 8, respectively. Within a similar electrostatic approach (assuming zero electron temperature in the channel), we also calculated the equilibrium electron density in 2*D* channel over the structure period when one or the other grating gate is biased to its threshold voltage (see Fig. 5). It is seen in Fig. 5 that the channel can be depleted under almost entire gate finger *G*2 while only small portion of the channel is depleted under gate finger *G*1.

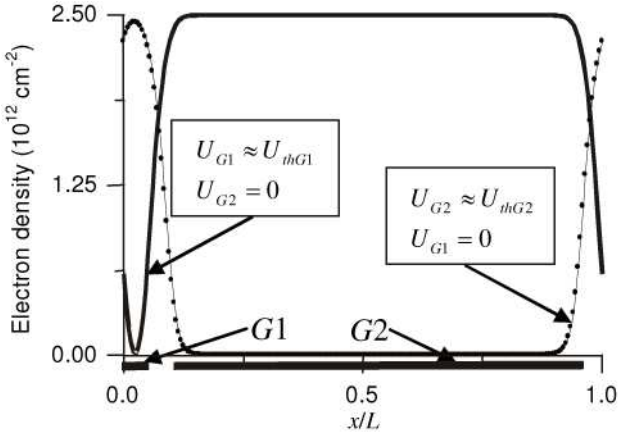

Fig. 5. Equilibrium electron density profile in biased structures over the structure period, *L*. Location of the grating-gate fingers is indicated by thick black bars under the abscissa axes. The origin is located under the edge of the *G*1 finger.

If we assume that the photovoltaic response is caused by slight lateral shift between the two different grating gates *G*1 and *G*2, the electric field at opposite ends of the depleted region of the channel would be also slightly different. Then we can characterize the photoresponse for different samples by estimating the detection length in the region of strong electric field having length Δ/4 at one end of the depleted part of the channel. Because of a very short depleted region under gate *G*1, one has $w \ll \Delta/4$ for samples # 1-4 and, hence, Eq. (3) yields

#119947 - $15.00 USD Received 13 Nov 2009; revised 18 Dec 2009; accepted 18 Dec 2009; published 11 Mar 2010

$$L_D \approx \pi \left| \frac{E_x}{E_0} \right|^2 \frac{w}{\Delta} w \tag{4}$$

for those samples. In the last formula the ratio w/Δ is the form-factor describing a fraction of Δ occupied by the depleted portion of the channel. For samples # 5-8, the whole region of strong electric field is depleted so that one has $w \approx \Delta/4$ and, hence,

$$L_D \approx \left| \frac{E_x}{E_0} \right|^2 \frac{\Delta}{4\pi} \tag{5}$$

in this case. Calculated detection lengths for all eight different samples shown in Fig. 6 demonstrate good agreement with the measured photoresponse for all samples.

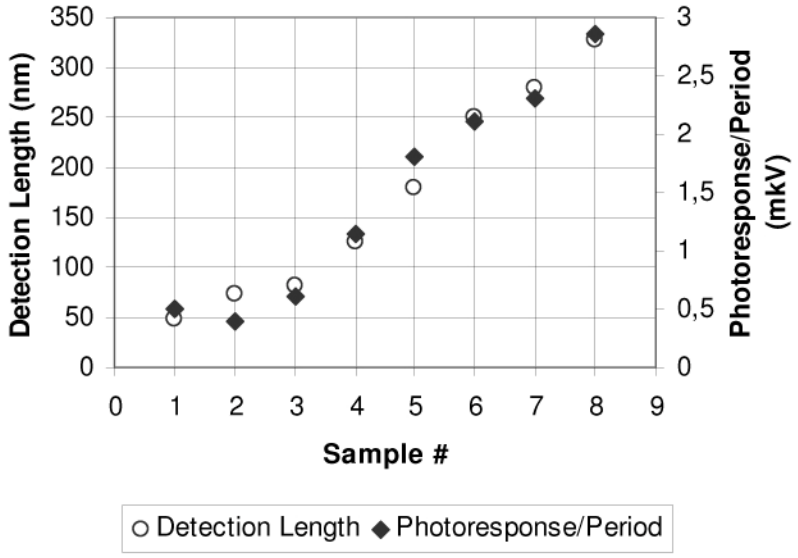

Fig. 6. Calculated detection length (open circles) and measured photoresponse (solid diamonds) for different samples under different bias conditions.

The only fitting parameter to match the detection length dependencies for samples # 1-4 and those for samples # 5-8 is the length of the depleted region of $2D$ channel in samples # 1-4, which was assumed to be $2w \approx 25$ nm. This is a reasonable value taking into consideration extremely short depleted region of the channel under gate finger $G1$ that is demonstrated in Fig. 5.

4. Conclusions

We have measured a room temperature THz photovoltaic response in double-grating-gate InGaP/InGaAs/GaAs transistors and clearly show that the photoresponse is due to hydrodynamic nonlinearity of 2D electron fluid in the channel and that the main part this photoresponse is coming from depleted regions of the channel. Strong THz-electric-field enhancement factor achieved in the double-grating-gate structure was demonstrated. Our results allow us to predict the high responsisivity of the double gate grating structures with a designed asymmetric unit cell.

Acknowledgments

This work has been supported by the GDR-E project “Semiconductor Sources and Detectors for Terahertz Frequencies” and PHC SAKURA “Research and Development of Terahertz Plasma-wave Transistors”. The work at the Université Montpellier2 and CNRS was supported

#119947 - $15.00 USD Received 13 Nov 2009; revised 18 Dec 2009; accepted 18 Dec 2009; published 11 Mar 2010

by the Region of Languedoc-Roussillon “Terahertz Platform”. The work at the Kotelnikov Institute was supported by the Russian Foundation for Basic Research (Grant Nos. 08-02-92497 and 09-02-00395) and from the Russian Academy of Sciences Program “Fundamentals of Nanotechnology and Nanomaterials”. The work at the Tohoku University was supported by the SCOPE Program from the MIC, Japan, and by the Grant in Aid for Basic Research (S) from the JSPS, Japan. YMM thanks the Ramon y Cajal Programme, Spain, for support.

#119947 - $15.00 USD Received 13 Nov 2009; revised 18 Dec 2009; accepted 18 Dec 2009; published 11 Mar 2010